Published in IET Microwaves, Antennas & Propagation
Received on 29th July 2008
Revised on 5th February 2009
doi: 10.1049/iet-map.2008.0258

ISSN 1751-8725

Ultra-wideband power dividers with good isolation and improved sharp roll-off skirt

S.W. Wong L. Zhu

School of Electrical and Electronics Engineering, Nanyang Technological University, 50 Nanyang Avenue, Singapore 639798, Singapore
E-mail: wong0342@ntu.edu.sg

Abstract: A novel class of ultra-wideband power dividers with good isolation and sharp roll-off skirt is proposed, analysed and designed on microstrip topology. By introducing a pair of quarter-wavelength short-circuited stubs and/or parallel coupled lines to two symmetrical output ports, good performance in terms of equal power splitting is achieved over the ultra-wideband range, that is 3.1–10.6 GHz. A single resistor is then placed between two output ports such that good isolation is achieved between them. By virtue of direct-current chocked and half-wavelength transmission zeros of short-circuited stubs and coupled lines, out-of-band roll-off skirt near the cut-off frequencies is sharpened to a great extent. Two types of these power dividers are analysed and optimised using the simple transmission-line based even- and odd-mode approach. Based on comparative study of these two types, an ultra-wide band divider with coupled lines has been designed and fabricated. Measured results evidently confirm the predicted features of the divider in terms of return losses at all the three ports, input-to-output insertion losses and output-to-output isolation.

1 Introduction

Power dividers are one of the indispensable components in many microwave modules and subsystems such as antenna arrays, power amplifiers, mixers, phase shifters and so on. The simplest and useful power divider is the Wilkinson divider with excellent isolation between two output ports at the centre frequency [1]. However it has only 20% fractional bandwidth for the single-stage case. Owing to the growth of unlicensed use of ultra-wideband (UWB) for short-distance indoor and hand-held wireless communications, there has been a tremendously raised interest in exploration of various UWB components that operate in a frequency range of 3.1–10.6 GHz. For this purpose, a few types of wideband power dividers [2–8] have been recently proposed. The most straightforward approach to construct such a wideband power divider is to cascade several multi-stage matching/isolating networks at two output ports of a single Wilkinson divider. However this approach dramatically increases the overall circuit size and requires more resistors for good isolation. According to the analysis in [2] for a multi-stage Wilkinson divider, at least three sections and three resistors are needed to achieve the desired UWB frequency response. In [3], a multi-section impedance transformer was placed at the input port of a multi-way junction to obtain good wideband return loss, but this divider suffers from poor isolation because of absence of a resistor between any of its two outputs. In [4], three-stage wideband Wilkinson power divider was explored for differential application. In [5], three-stage wideband Wilkinson power divider was presented with an arbitrary power division ratio between two output ports. Recently, special attention has been shifted to exploration of UWB power dividers with the operating band in the overall 3.1–10.6 GHz UWB region. In [6], an out-of-phase UWB power divider is implemented with microstrip to slotline transition. In [7], a wideband divider is formed with broadside coupling structure.

In this paper, a novel class of UWB power dividers based on single-layer microstrip topology is proposed, analysed and designed. Following the basic idea of the design of UWB bandpass filters in [9, 10], quarter-wavelength short-circuited stubs and/or parallel coupled lines are placed at the two output ports of a traditional single-stage Wilkinson divider. The expected UWB power-splitting performance can be realised with good impedance matching at the input

port and 3-dB power transmission from the input to the two output ports. Since a resistor is placed between two output ports, good isolation can be achieved in the overall UWB region. Our proposed designs carry several attractive features that include size compactness with $0.39\lambda^2$ in area (λ is the guided wavelength at centre frequency), high in-band selectivity, sharp roll-off skirt, less resistors (required only one isolation resistor while others [2, 4, 5] require several of them) and easy for fabrication on single-layer PCB technology. In the remainder of this work, a transmission-line-based approach is presented under even- and odd-mode excitations to analyse and optimise the design of the proposed UWB power dividers. In this work, the power divider with coupled-line sections is optimised by using the circuit simulator in Agilent ADS software. A prototype power divider is then designed and fabricated on the RT/Duroid 6010 substrate with a dielectric constant of 10.8, loss tangent of 0.0023 and thickness of 0.635 mm. Predicted results with good power splitting and isolation performances over the UWB are experimentally verified.

2 UWB power divider without coupled-line section

The schematic of the first proposed power divider namely, Type-A, is shown in Fig. 1*a*. The overall design is different from the traditional multi-stage Wilkinson power divider [4]. Two pairs of quarter-wavelength short-circuited stubs are symmetrically placed at the two outputs and they are joined through a pair of quarter-wavelength impedance transformer. Effectively, each arm of the divider includes a circuit that is similar to the two-port UWB bandpass filter with short-circuited stubs [8]. In principle, it is thus possible to achieve an UWB power splitting performance by properly designing the two individual impedance transformers with the characteristic impedance of Z_1 and Z_2 as well as the two identical short-circuited stubs with the characteristic impedance of Z_3. Moreover, different from the two existing UWB power dividers [6, 7] with poor isolation, a single resistor R is placed between two output parts and its value is properly selected to attain good isolation between port 2 and port 3 over the required UWB range.

2.1 Odd-mode analysis

Fig. 1*b* shows the two-port transmission-line model for a symmetrical bisection of the UWB power divider in Fig. 1*a* under odd-mode excitation. In this case, port 1 can be simply form a short circuit since the strip conductor of this port is grounded by the virtual electric wall. The model becomes a one-port network as shown in Fig. 1*b*, and the input admittance at port 2 can be derived as

$$Y^{o}_{in2} = Y_2 \frac{Y^{o}_{t} + jY_2 \tan(\theta)}{Y_2 + jY^{o}_{t} \tan(\theta)} - jY_3 \cot(\theta) \quad (1)$$

where $Y^{o}_{t} = 2/R - jY_3\cot(\theta) - jY_1\cot(\theta)$.

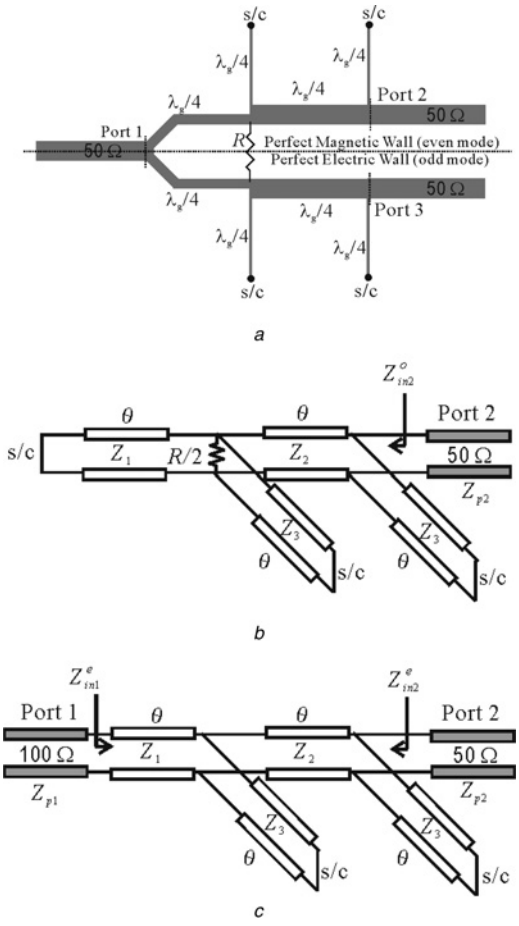

Figure 1 *Proposed UWB microstrip power divider without coupled line, namely, Type-A*

a Schematic
b Odd-mode model
c Even-mode model

As illustrated in Fig. 1*b*, $Z_{p2} = 1/Y_{p2} = 50\ \Omega$ represents the port impedance at port 2 of the odd-mode bisection. At the centre frequency of UWB, that is 6.85 GHz, $\theta = \pi/2$ and $Y^{o}_{in2} = Y_{p2}$ implies no reflection at port 2. Thereafter (1) can be simplified as

$$R = \frac{Z_2^2}{0.5 Z_{p2}} \quad (2)$$

Equation (2) gives a simple guideline in selection of R. For an instance, if $Z_2 = 50\ \Omega$, $R = 100\ \Omega$, is obtained.

2.2 Even-mode analysis

Under the even-mode excitation, a symmetrical bisection of the three-port divider can be represented by a two-port network shown in Fig. 1*c*. Herein, the centre vertical plane becomes a perfect magnetic wall. The port impedance at port 1 is doubled, that is $Z_{p1} = 100\ \Omega$, since its relevant strip conductor is cut into halves. For the two-port network in Fig. 1*c*, the input admittances at port 1 and port 2 can be derived on a basis of the transmission-line theory and

doi: 10.1049/iet-map.2008.0258

they are expressed as

$$Y^{e}_{in1} = Y_1 \frac{Y^{e}_{t1} + jY_1 \tan(\theta)}{Y_1 + jY^{e}_{t1} \tan(\theta)} \quad (3)$$

$$Y^{e}_{in2} = Y_2 \frac{Y^{e}_{t2} + jY_2 \tan(\theta)}{Y_2 + jY^{e}_{t2} \tan(\theta)} - jY_3 \cot(\theta) \quad (4)$$

where

$$Y^{e}_{t1} = Y_2[Y^{e}_{t} + jY_2 \tan(\theta)]/[Y_2 + jY^{e}_{t} \tan(\theta)] - jY_3 \cot(\theta)$$

$$Y^{e}_{t} = Y_{p2} - jY_3 \cot(\theta)$$

$$Y^{e}_{t2} = Y_1[Y_{p1} + jY_1 \tan(\theta)]/[Y_1 + jY_{p1} \tan(\theta)] - jY_3 \cot(\theta)$$

To achieve good impedance matching at port 1 and port 2, $Y^{e}_{in1} = Y_{p1}$ and $Y^{e}_{in2} = Y_{p2}$ need to be restricted to an acceptable extent. Under this constraint, one can simplify (3) and (4) as a unified expression at the frequency of $\theta = \pi/2$

$$Z_1^2 = \frac{Z_2^2 Z_{p1}}{Z_{p2}} \quad (5)$$

Since $Z_{p1} = 100\ \Omega$ and $Z_{p2} = Z_2 = 50\ \Omega$ in this even-mode case, one can determine $Z_1 = 70.7\ \Omega$ from (5). It should be emphasised that (2) and (5) are only exactly valid at $\theta = \pi/2$ and impedance matching may be gradually degraded as θ deviates away from $\pi/2$. It is the same case as the traditional Wilkinson power divider [1]. Nevertheless, when short-circuited stubs are placed as shown in Fig. 1*a*, two additional transmission poles can be generated at the two sides of $\theta = \pi/2$. Good impedance matching can be achieved in the overall UWB region if these three poles are properly allocated as discussed in [8].

2.3 S-parameters analysis

As the input admittances at port 2 and port 3 are derived in (1), (3) and (4) for even- and odd-mode cases, the resultant S-parameters, S_{11} and S_{22}, can be expressed as

$$S_{11} = \frac{Y_{p1} - Y^{e}_{in1}}{Y_{p1} + Y^{e}_{in1}} \quad (6)$$

$$S_{22} = \frac{1}{2}\left(\frac{Y_{p2} - Y^{e}_{in2}}{Y_{p2} + Y^{e}_{in2}} + \frac{Y_{p2} - Y^{o}_{in2}}{Y_{p2} + Y^{o}_{in2}}\right) \quad (7)$$

With these two closed-form equations, frequency response of S-parameters can be calculated for the desired frequency range. Fig. 2 shows the calculated S-parameter magnitudes, that is $|S_{11}|$, $|S_{22}|$, $|S_{21}|$ and $|S_{32}|$ of the three-port power divider in Fig. 1*a* using the impedance of $Z_3 = 90\ \Omega$ and varied values of $Z_2 = 40$, 50 and 60 Ω. Comparing the cases of $Z_2 = 40$ and 60 Ω in Fig. 2*a*, the selection of $Z_2 = 50\ \Omega$ provides a better matching at port 1 over a very wide bandwidth. As shown in Fig. 2*b*, the selection of $Z_2 = 50\ \Omega$ achieves a good isolation and matching at port 2. Thus, we can conclude that $Z_2 = 50\ \Omega$ is the best value of them for this power divider. In this case, the fractional bandwidths under the definitions of 3-dB $|S_{11}|$ and $|S_{22}|$ are found to be

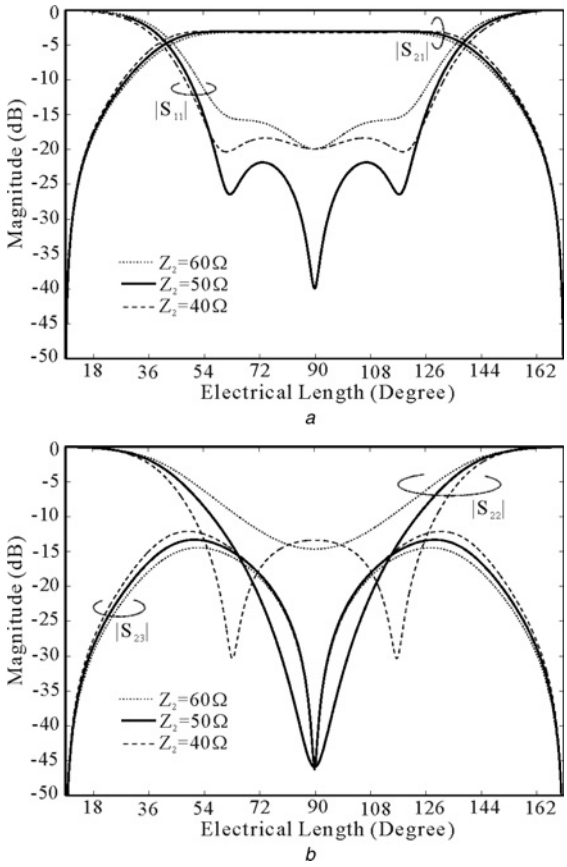

Figure 2 *Simulated S-parameters with respect to electrical length (θ) for the Type-A UWB power divider with varied values of $Z_2 = 60$, 50 and 40 Ω*

a S_{21}- and S_{11}-parameters
b S_{23}- and S_{22}-parameters

about 129 and 121%, respectively. Meanwhile, we can find that $|S_{21}|$ achieves very flat 3-dB power splitting performance in the frequency band of 121% fractional bandwidth and sharp roll-off skirt near the lower and upper cut-off frequencies. This excellent transmission performance with 3-dB return loss in the UWB is mainly brought out by the two in-band transmission poles of two pairs of short-circuited stubs. Different from [6, 7], $|S_{32}|$ in Fig. 2 is lower than −13 dB over the plotted frequency range as the resistor of $R = 100\ \Omega$ is introduced. Thus, the power divider not only shows excellent return and insertion losses but also attains reasonably good isolation in the overall UWB band with the fractional bandwidth of 121%.

3 Power divider with coupled-line section

In this section, an alternative UWB power divider, namely, Type-B, is presented with the target of improved out-of-band performance. Fig. 3*a* shows its schematic diagram. In comparison to the initial UWB divider in Fig. 1*a*, the pair of impedance transformers of Type-A has been replaced by a pair of high-impedance coupled-lines and the resulting design is named as Type-B divider. As discussed in [9],

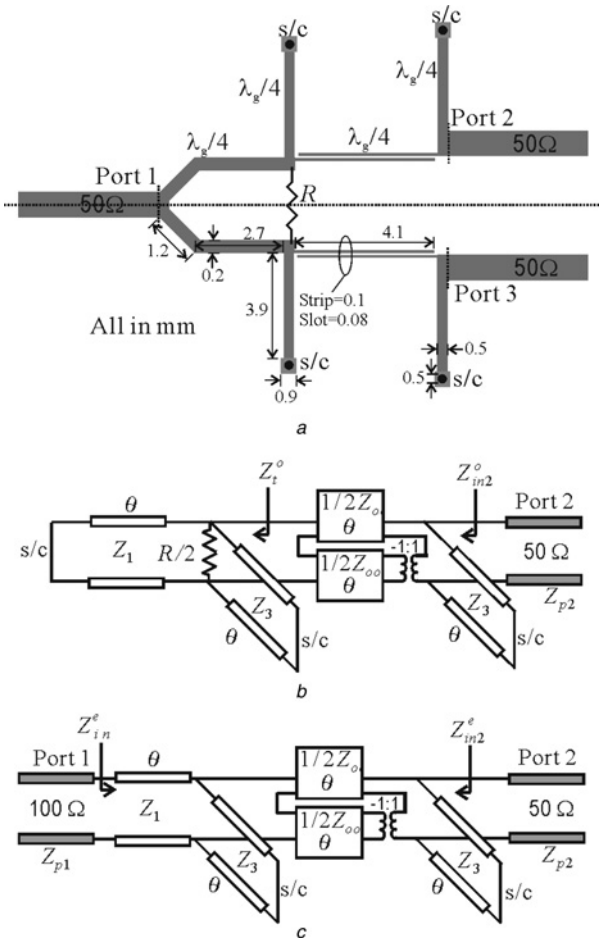

Figure 3 *Proposed UWB microstrip power divider with coupled line, namely, Type-B*

a Schematic with all dimensions
b Odd-mode model
c Even-mode model

the introduction of these coupled-lines renders two additional transmission poles in the UWB. In principle, the roll-off skirts near the lower and upper cut-off frequencies can be effectively sharpened since the total number of transmission poles is increased inside the UWB. For analysis, the two modified equivalent models are formulated under the odd- and even- mode excitations. Figs. 3*b* and *c* depict these models, where the equivalent models of coupled-line section is derived based on the coupled-line theory [11]. Proceeding with the similar analysis in Section 2, (1)–(5) can be modified as (8)–(12) imposing the constraints of 3-dB $|S_{21}|$ as well as minimum $|S_{11}|$, $|S_{22}|$ and $|S_{32}|$.

In the odd-mode case, the input admittance at port 2 in Fig. 3*b* can be derived as

$$Y^{o}_{in2} = \frac{4j + 2Y^{o}_{t} Z_{+} \cot(\theta)}{2Z_{+}\cot(\theta) + jY^{o}_{t} Z^{2}_{-} \csc^{2}(\theta) - jY^{o}_{t} Z^{2}_{+} \cot^{2}(\theta)} - jY_3 \cot(\theta) \quad (8)$$

where $Y^{o}_{t} = 2/R - jY_3\cot(\theta) - jY_1\cot(\theta)$, $Z_{-} = Z_{oe} - Z_{oo}$ and $Z_{+} = Z_{oe} + Z_{oo}$. Z_{oe} and Z_{oo} are the even- and odd-mode characteristic impedances of the coupled-line section, respectively.

Based on the equivalent even-mode network in Fig. 3*c*, the input admittance at port 1 can be obtained as

$$Y^{e}_{in1} = Y_1 \frac{Y^{e}_{t1} + jY_1 \tan(\theta)}{Y_1 + jY^{e}_{t1} \tan(\theta)} \quad (9)$$

where

$$Y^{e}_{t1} = \frac{4j + 2Y^{e}_{t} Z_{+} \cot(\theta)}{2Z_{+}\cot(\theta) + jY^{e}_{t} Z^{2}_{-} \csc^{2}(\theta) - jY^{e}_{t} Z^{2}_{+} \cot^{2}(\theta)} - jY_3 \cot(\theta)$$

$$Y^{e}_{t} = Y_{p2} - jY_3 \cot(\theta)$$

and the input admittance at port 2 becomes

$$Y^{e}_{in2} = \frac{4j + 2Y^{e}_{t2} Z_{+} \cot(\theta)}{2Z_{+}\cot(\theta) + jY^{e}_{t2} Z^{2}_{-} \csc^{2}(\theta) - jY^{e}_{t2} Z^{2}_{+} \cot^{2}(\theta)} - jY_3 \cot(\theta) \quad (10)$$

where

$$Y^{e}_{t2} = Y_1 \frac{Y_{p1} + jY_1 \tan(\theta)}{Y_1 + jY_{p1} \tan(\theta)} - jY_3 \cot(\theta)$$

Similar to the analysis approach in Section 2, the good impedance matching constraint at all the three ports at the frequency of $\theta = \pi/2$ leads to derivative of the following two closed-form formulae

$$R = \frac{Z^{2}_{-}}{2Z_{p2}} \quad (11)$$

$$Z^{2}_{1} = \frac{Z_{p1} Z^{2}_{-}}{4Z_{p2}} \quad (12)$$

It should be noted that both two-way power dividers have $Z_{p2} = Z_{p3} = 50\,\Omega$. Based on (11), if $R = 100\,\Omega$ is selected, we can obtain $Z_{-} = 100\,\Omega$, where $Z_{oe} = 135\,\Omega$ and $Z_{oo} = 35\,\Omega$. Similar to the Type-A divider, the port impedances at port 1 and port 2 become $Z_{p1} = Z_{-} = 100\,\Omega$ and $Z_{p2} = 50\,\Omega$. Thus, from (12), we can calculate $Z_1 = 70.7\,\Omega$, under the constraint of good return/insertion losses, $Z_3 = 60\,\Omega$ for the short-circuited stubs can be determined.

Fig. 4 plots the calculated S-parameter magnitudes over a wide range of electrical length (θ) that is quasi-linearly proportional to frequency. From (11) and (12), we can derive a matching condition, that is $Z_{-} = 100\,\Omega$ where $Z_{-} = Z_{oe} - Z_{oo}$. In order to obtain a set of optimised value of Z_{oe} and Z_{oo}, three sets of Z_{oe} and Z_{oo} are plotted

doi: 10.1049/iet-map.2008.0258

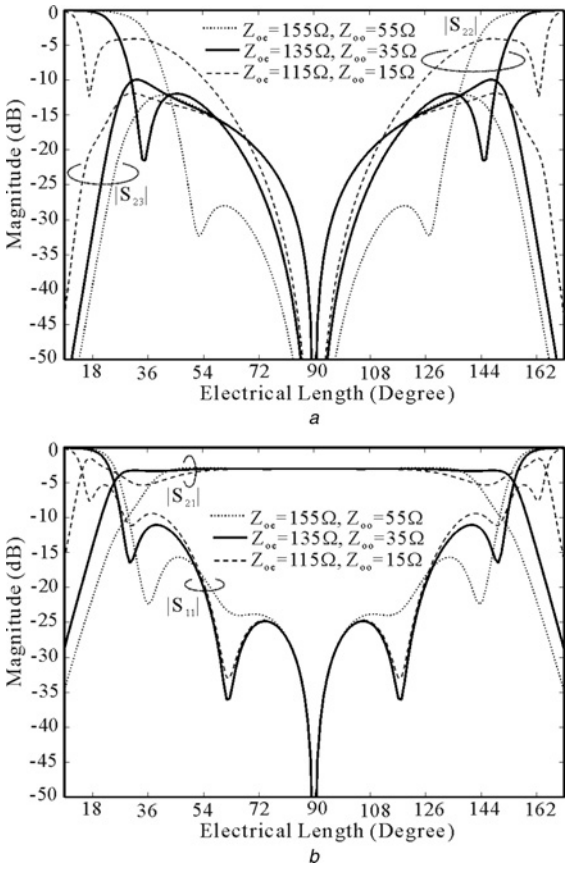

Figure 4 *Simulated S-parameters with respect to electrical length (θ) for the Type-B UWB power divider with varied values of (Z_{oe}, Z_{oo}) = (115 Ω, 15 Ω), (135 Ω, 35 Ω) and (155 Ω, 55 Ω), respectively*

a S_{21}- and S_{11}-parameters
b S_{23}- and S_{22}-parameters

in Figs. 4*a* and *b*. As can be seen in Fig. 4*a*, the set with $Z_{oe} = 155\ \Omega$ and $Z_{oo} = 55\ \Omega$ has narrow bandwidth matching at port 1 and some undesired $|S_{21}|$ spurious appear near the cut-off region. The set with $Z_{oe} = 115\ \Omega$ and $Z_{oo} = 15\ \Omega$ has very good matching at port 1 and sharp rejection skirt for the $|S_{21}|$, but the bandwidth is not wide enough to cover the desired passband. Comparatively, the set with $Z_{oe} = 135\ \Omega$ and $Z_{oo} = 35\ \Omega$ can be considered as the best values as it has a good wideband matching at port 1 with return loss larger than 10 dB and sharp rejection at the cut-off region. Now let us look at Fig. 4*b*, the isolations $|S_{23}|$ change slightly when three sets of the Z_{oe} and Z_{oo} are considered. However, the set with $Z_{oe} = 135\ \Omega$ and $Z_{oo} = 35\ \Omega$ has wider bandwidth for the port 2 matching when compares with other two sets of Z_{oe} and Z_{oo}, so we conclude that the set with $Z_{oe} = 135\ \Omega$ and $Z_{oo} = 35\ \Omega$ is the best values for this power divider. Since the coupled line generates two additional transmission zeros at $\theta = 0$ and π [9]. The roll-off skirt of Type-B divider is obviously sharper than that of the Type-A counterpart if two sets of graphs in Figs. 2 and 4 are compared (solid lines). From Fig. 4, we can find that the fractional bandwidth is 135% which is slightly wider than the 121% bandwidth observed in case of Type-A divider. Moreover, all of $|S_{11}|$, $|S_{22}|$ and $|S_{32}|$ are lower than −10 dB and $|S_{21}|$ is close to −3 dB over the desired UWB passband.

4 Discussion and experimental verification

So far, the two UWB power dividers have been individually analysed and designed. To comparatively investigate their UWB power splitting performances, the lower/upper cut-off frequencies can be calculated via (6) and (7) under the 3-dB bandwidth definition for $|S_{11}|$ and $|S_{22}|$. Figs. 5*a* and *b* illustrate the calculated electrical lengths or phases (θ) at the two cut-off frequencies against characteristic impedance (Z_3) of short-circuited stubs for the Type-A and Type-B dividers. As pointed out in Sections 2 and 3, the fractional

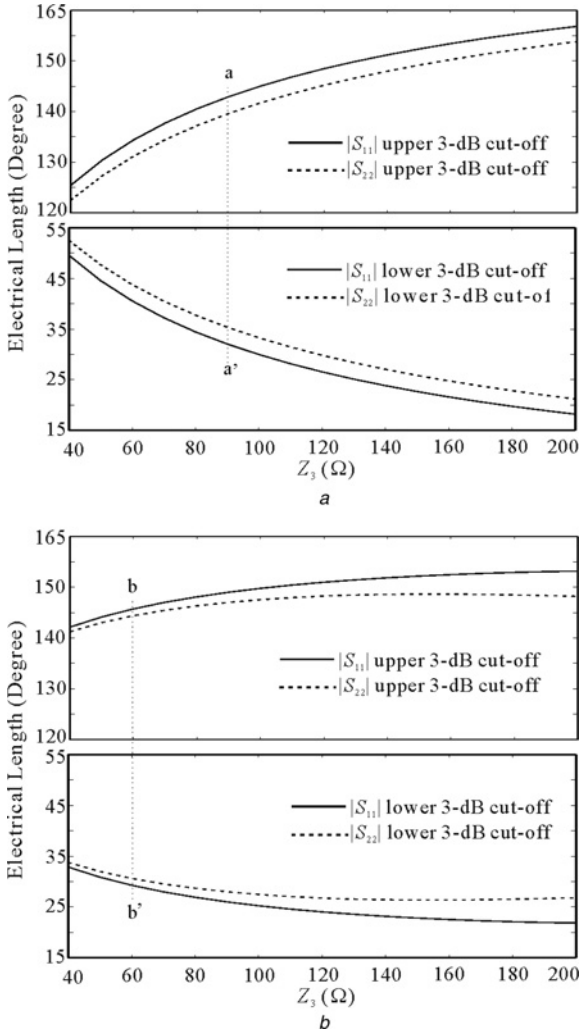

Figure 5 *Electrical length (θ) of lower and upper cut-off frequencies against characteristic impedance (Z_3) of short-circuited stubs for the two proposed UWB power dividers in Figs. 1 and 3*

a Type-A
b Type-B

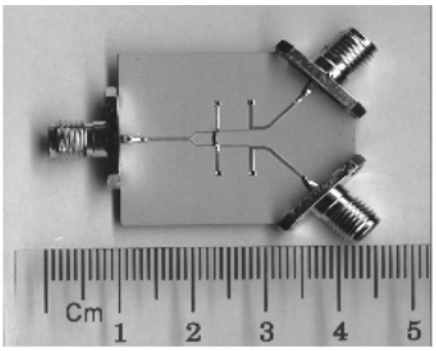

a

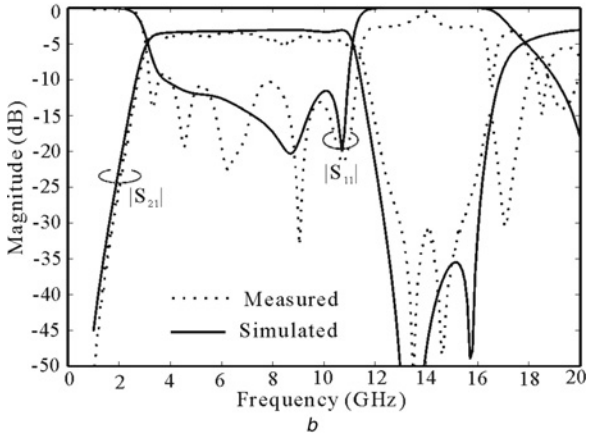

b

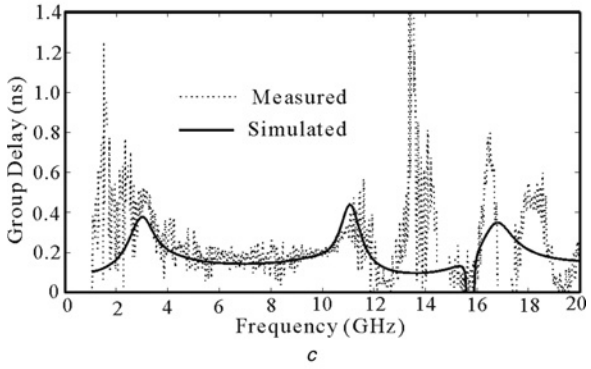

c

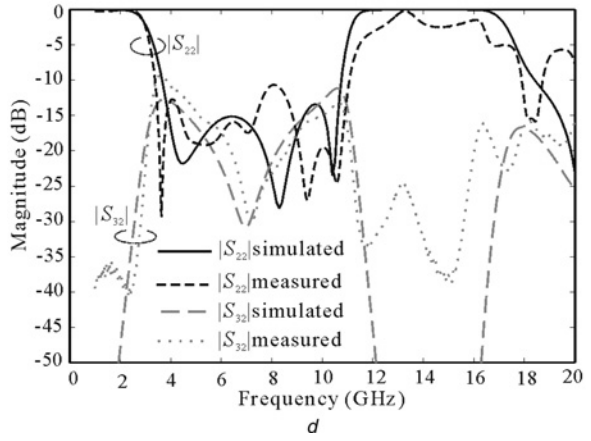

d

Figure 6 *Predicted and measured results of the designed UWB power divider*

a Photograph
b S_{21}- and S_{11}-magnitudes
c Group delay
d S_{22}- and S_{32}-magnitudes

bandwidths of these two power dividers can be expressed as the difference of the upper/lower phases (θ) over its central value since θ is linearly proportional to the frequency (f).

With reference to Fig. 5*a*, these two cut-off phases (θ) are found to go up and down simultaneously as Z_3 increases from 40 to 200 Ω, progressively enlarging the spacing between them or widening the operating frequency bandwidth. So the bandwidth of the Type-A divider can be easily varied with virtue of adjustment of Z_3. In Fig. 5*a*, the dotted straight line (a–a′) represents the case of $Z_3 = 90\ \Omega$ (Fig. 2) and its interception points with two sets of θ-curves allow us to calculate the fractional bandwidths, that is 129 and 121% for $|S_{11}|$ and $|S_{22}|$ as discussed in Section 2. Now, let us consider Fig. 5*b* for the Type-B divider. The bandwidth for $|S_{11}|$ is still wider than that for $|S_{22}|$ in this coupled-line case. Owing to the presence of two additional transmission poles in this case, its upper and lower cut-off phases (θ) become larger and smaller than those of its counterpart Type-A if the impedance Z_3 is unchanged. The fractional bandwidth of this Type-B divider can be further enlarged if necessary. With the target of the same bandwidth as that in the Type-A, we can determine $Z_3 = 60\ \Omega$ that is represented by the b–b′ dotted line in Fig. 5*b*.

As the two UWB dividers are designed in Sections 2 and 3, a prototype UWB divider based on the improved structure in Fig. 3*a* is fabricated and measured. Fig. 6*a* is the photograph of the fabricated UWB power divider with the three SMA connectors at three ports. Fig. 6*b* shows the predicted S_{21}- and S_{11}-magnitudes as well as the group delay in comparison to the measured results. They are in reasonably good agreement with each other over the frequency range from 1 to 20 GHz, exhibiting good performance in terms of 3-dB power splitting. The simulated in-band insertion loss is less than 3.3 dB. The return loss is higher than 10.0 dB over the desired passband and its roll-off skirt near the lower and cut-off frequencies, that is 3.1 and 10.6 GHz, has been effectively sharpened as expected in theory. The spurious passband is observed in the frequencies higher than 16.5 GHz and it is primarily due to the periodic harmonics of coupled lines and short-circuited stubs as also existed in [8, 9]. The group delay of $|S_{21}|$ is about 0.19 ns at the central frequency of the UWB and it is very flat over the passband. This implies good linearity of this power divider within the operation frequency range. Fig. 6*c* illustrates the comparison between the predicted and measured S_{22}- and S_{32}-magnitudes. Again, they are in good agreement with each other. The return loss at port 2 and port 3 as well as the isolation between port 2 and port 3 are all higher than 10 dB over the realised UWB band.

5 Conclusion

This paper has presented a class of UWB power dividers with good isolation between two output ports and sharp out-of-

IET Microw. Antennas Propag., 2009, Vol. 3, Iss. 8, pp. 1157–1163
doi: 10.1049/iet-map.2008.0258

band roll-off skirt. A simple approach based on the equivalent circuit models under the even- and odd-mode excitations has been developed for efficient analysis and design of two UWB power dividers. It is demonstrated that as two pairs of short-circuited stubs are introduced via an impedance transformer, three poles can be introduced in the UWB. As this transformer is replaced by the coupled line, two additional poles can be further excited. After comparative study of the two dividers, the divider with a pair of coupled lines is found to achieve much sharper roll-off skirt. A prototype UWB divider is designed and fabricated. Measured results have confirmed the predicted power splitting performance with the 3-dB power transmission from one input to two outputs, good impedance matching at all the three ports and good isolation between two outputs over the 3.1-to-10.6 GHz UWB band.

6 References

[1] WILKINSON E.: 'An N-way hybrid power divider', *IRE Tran. Microw. Theory Tech.*, 1960, **8**, (1), pp. 116–118

[2] LEE S.W., KIM C.S., CHOI K.S., PARK J.S., AHN D.: 'A general design formula of multi-section power divider based on singly terminated filter design theory', *IEEE Microw. Symp. Dig.*, 2001, **2**, pp. 1297–1300

[3] KISHIHARA M., YAMANE K., KAWAI T.: 'A design of multi-stage, multi-way microstrip power dividers with broadband properties', *IEEE Microw. Wirel. Compon. Lett.*, 2004, **1**, pp. 69–72

[4] CHIU L., YUM T.Y., XUE Q., CHAN C.H.: 'A wideband compact parallel-strip 180° Wilkinson power divider for push–pull circuitries', *IEEE Microw. Wirel. Compon. Lett.*, 2006, **16**, pp. 49–51

[5] ORAIZI H., SHARIFI A.-R.: 'Design and optimization of broadband asymmetrical multisection wilkinson', *IEEE Trans. Microw. Theory Tech.*, 2006, **54**, pp. 2220–2231

[6] BIALKOWSKI M.E., ABBOSH A.M.: 'Design of a compact UWB out-of-phase power divider', *IEEE Microw. Wirel. Compon. Lett.*, 2007, **17**, pp. 289–291

[7] ABBOSH M.: 'A compact UWB three-way power divider', *IEEE Microw. Wirel. Compon. Lett.*, 2007, **17**, pp. 598–600

[8] WONG S.W., ZHU L.: 'Ultra-wideband power divider with good in-band splitting and isolation performances', *IEEE Microw. Wirel. Compon. Lett.*, 2008, **18**, pp. 518–520

[9] SHAMAN H., HONG J.-S.: 'A novel ultra-wideband (UWB) bandpass filter (BPF) with pairs of transmission zeroes', *IEEE Microw. Wirel. Compon. Lett.*, 2007, **17**, (2), pp. 121–123

[10] ZHU L., SUN S., MENZEL W.: 'Ultra-wideband (UWB) bandpass filters using multiple-mode resonator', *IEEE Microw. Wirel. Compon. Lett.*, 2005, **15**, (11), pp. 796–798

[11] ZYSMAN G.L., JOHNSON A.K.: 'Coupled transmission line networks in an inhomogeneous dielectric medium', *IEEE Trans. Microw. Theory Tech.*, 1969, **17**, (10), pp. 753–759

doi: 10.1049/iet-map.2008.0258